

Development of a High-Time-Resolution Detector Utilizing Novel Scintillators for Neutral Hadron Momentum Measurement

Xiyang Wang^a, Hongyu Zhang^a, Shiming Zou^a, Zibing Bai^c, Deqing Fang^{a,b,*}, Kairui Huang^a, Ziyu Liu^c, Yugang Ma^{a,b,*}, Weiqi Meng^c, Ting Wang^a, Xiaolong Wang^{a,*}, Shiqing Xie^a, Mingjie Yang^a, Junhao Yin^c, Mingkuan Yuan^a, Wanyi Zhuang^a

^aKey Laboratory of Nuclear Physics and Ion-beam Application (MOE) and Institute of Modern Physics, Fudan University, 220 Handan Road, Shanghai, 200433, China

^bShanghai Research Center for Theoretical Nuclear Physics, NSFC and Fudan University, Shanghai, 200438, China

^cSchool of Physics, Nankai University, 94 Weijin Road, Nankai District, Tianjin, 300071, China

Abstract

Accurate momentum determination of neutral hadrons, such as K_L mesons and neutrons, remains a significant challenge in particle and nuclear physics experiments. The Belle II experiment, equipped with a large K_L and Muon Detector (KLM), presents an opportunity to address this challenge through an upgrade incorporating Time-of-Flight capability for direct momentum measurement of long-lived neutral hadrons. We investigate the feasibility of such an upgrade, focusing on the conceptual design for momentum determination via TOF measurements. We propose the use of cost-effective plastic scintillators with large attenuation lengths and large-area silicon photomultipliers (SiPMs) to achieve high time resolution. Research and development efforts are reported on developing new scintillators and the implementation of compact $6\text{ mm} \times 6\text{ mm}$ SiPM arrays to enhance photon collection efficiency. Scintillator samples with a cross section of $4\text{ cm} \times 2\text{ cm}$ and varying lengths (50 cm, 100 cm, 135 cm, and 150 cm) are studied. A bulk attenuation length of $120 \pm 7\text{ cm}$ has been achieved with the 135 cm-long sample, along with a time resolution of $70 \pm 7\text{ ps}$ at its midpoint. The 50 cm scintillator demonstrates an exceptional time resolution of $47 \pm 2\text{ ps}$. These results highlight the potential of the proposed technology for improving neutral hadron momentum measurements in the upgraded Belle II KLM detector.

Keywords: Time-of-Flight, Time resolution, Muon detector, Scintillator, SiPM

1. Introduction

In particle and nuclear physics experiments, accurately determining the momentum of neutral hadrons, such as K_L mesons and neutrons, poses significant challenges. High energy frontier experiments like ATLAS [1] and CMS [2] employ costly hadron calorimeters (HCALs) that achieve energy resolutions $\sigma(E)/E$ of approximately $(0.5 - 0.9)/\sqrt{E}$ [3, 4]. On the other hand, intensity frontier experiments such as BaBar [5], Belle [6], Belle II [7, 8], and BESIII [9] do not use HCALs for measuring the energy of neutral hadrons with momenta ranging from $1 - 5\text{ GeV}/c$. This is pri-

marily due to the limited energy resolution of HCALs can be achieved in this momentum region.

As a super B-factory experiment, the Belle II experiment was designed to explore new physics at the forefront of high-luminosity collisions and improve the precision of measurements for Standard Model parameters [10]. The Belle II spectrometer has a huge outermost subdetector, the K_L and Muon Detector (KLM) [8]. In the Conceptual Design Report (CDR) [11, 12] for the Belle II upgrade, we proposed enhancing the KLM system with a new capability: Time-of-Flight (TOF) measurements. This upgrade would allow for the direct determination of momentum for a long-lived neutral hadron based on its velocity. However, implementing TOF technology poses a significant challenge due to the need for cost-effectiveness, given the large volume and number of readout channels of the KLM system. Therefore, achieving this innova-

*Corresponding author

Email addresses: dqfang@fudan.edu.cn (Deqing Fang), mayugang@fudan.edu.cn (Yugang Ma), xiaolong@fudan.edu.cn (Xiaolong Wang)

tion requires a careful balance between advanced functionality and economic feasibility.

Traditional TOF detectors primarily rely on two technological approaches. The first approach employs plastic scintillators coupled with photomultiplier tubes (PMTs), as implemented in the Belle TOF [13] and BESIII TOF [14] systems. However, PMTs have inherent limitations, including their large physical size, which creates dead zones, and the requirement of a high-voltage (HV) system operating at over 1000 V. Additionally, the inherent transit time spread of PMTs makes achieving high time resolution (HTR) with excellent precision a significant challenge. Nevertheless, the use of such scintillators and PMTs also incurs significant costs. The second approach utilizes multi-gap resistive plate chambers (MRPCs), as seen in experiments such as STAR [15], ALICE [16], and the upgraded endcap TOF of BESIII [17]. While MRPCs can achieve an HTR of 50 – 60 ps, they suffer from notable drawbacks, including complex structures requiring gas flow systems, susceptibility to gas contamination (e.g., $C_2H_2F_4/C_4H_{10}/SF_6$), and a large number of readout channels. These limitations highlight the need for alternative technologies that balance performance, simplicity, and cost-effectiveness.

Silicon photomultipliers (SiPMs) coupled with new scintillators present a promising alternative for TOF detectors, offering HTR and insensitivity to magnetic fields. Currently, several experiments have successfully implemented SiPMs with small-sized scintillators (length ≤ 15 cm) to construct TOF systems, achieving time resolutions better than 100 ps, as demonstrated by the PANDA [18] and AMS-100 [19] experiments. However, the application of SiPMs with large, elongated scintillators remains limited. Key challenges in such implementations include the scintillator’s attenuation length, elevated noise levels in SiPM arrays, and issues associated with slow rise times (τ_{rise}). Addressing these challenges is crucial for extending the use of SiPM-based TOF systems for larger-scale applications.

This paper introduces an innovative scintillation detection approach that builds upon and enhances the foundational scheme developed for the Belle II KLM upgrade. Since 2018, our laboratory at Fudan University has been collaborating with the GaoNengKeDi Company [20] in Beijing to develop new scintillators optimized for HTR and low cost. We have significantly improved time resolution by improving scintillators with extended attenuation lengths and integrating a detection array featuring large-area SiPMs paired with ultrafast front-end electronic readouts. This advancement paves the way for more efficient and cost-effective

TOF systems in large-scale applications.

2. Belle II KLM and its upgrade

As the outermost component of the Belle II detector, the KLM is responsible for identifying K_L mesons and muons with momenta up to 4.5 GeV/c [7, 11]. As illustrated in Fig. 1(a), the KLM spans radii from 200 cm to 240 cm in the octagonal barrel region and from 130 cm to 340 cm in the endcaps. The barrel section consists of 15 detector layers interspersed with 14 layers of yoke iron, while each endcap contains 14 detector layers and 14 layers of iron. The yoke serves a dual purpose: it acts as a magnetic flux return for the solenoid and enables hadronic cascade clustering, which is essential for K_L detection.

The large-surface-area detector panels, approximately 3.1 cm thick, are positioned between 4.7 cm steel plates. Within these panels, the innermost two layers of the barrel and all layers of the endcaps are equipped with extruded scintillator detector modules, which achieve an intrinsic time resolution of around 1 ns per detection channel [21]. The remaining 13 barrel layers utilize the Belle experiment’s legacy Resistive Plate Chambers (RPCs). In the scintillator modules, each scintillator strip incorporates a Kuraray Y11(200)MSJ wavelength-shifting (WLS) fiber [22], which collects photons emitted by the extruded scintillator and guides them to a Hamamatsu (HPK) MPPC S10362-13-050C, a SiPM with a sensitive area of 1.3 mm \times 1.3 mm [29].

In the CDR of the Belle II upgrade [11], we proposed the idea of enhancing the KLM system with the capability to **measure the momenta of K_L mesons through a time-of-flight (T_{fly}) measurement using new scintillator detectors**. Figure 1(b) illustrates a hadronic cluster generated by a K_L meson, as visualized in the Belle II virtual reality simulation [23]. The simulation data reveal multiple hits within this hadronic cluster. Our Geant4-based simulations [24] of an upgraded KLM indicate that measuring the T_{fly} of a K_L meson is achievable by leveraging the rapid hits detected in this system [11].

The momentum p of a neutral hadron with a given velocity β is expressed as:

$$p = \gamma m v = \frac{m c \beta}{\sqrt{1 - \beta^2}} = \frac{m c L}{\sqrt{T^2 c^2 - L^2}}, \quad (1)$$

where γ is the Lorentz factor, m , L , and T_{fly} are the nominal mass, the flight length, and the flight time of this hadron. The relationship between the uncertainty in

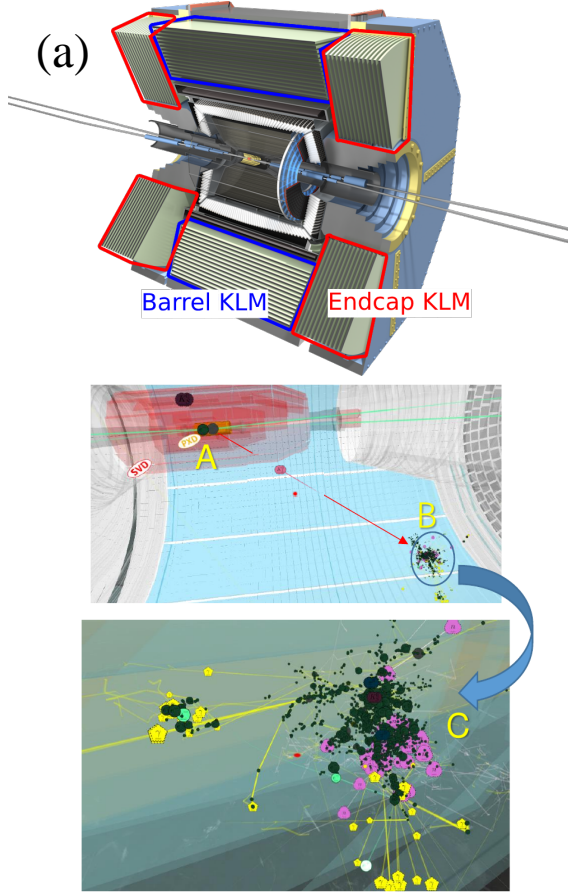


Figure 1: (a) The KLM in the Belle II detector and (b) a hadronic cluster generated by a K_L meson in the Belle II virtual reality.

momentum, $\sigma(p)$, and the uncertainty in time of flight, $\sigma(T_{\text{fly}})$, is given by:

$$\frac{\sigma(p)}{p} = \frac{T_{\text{fly}} p^2}{m^2 L^2} \cdot \sigma(T_{\text{fly}}). \quad (2)$$

In practical measurements, the ratio L/T_{fly} is approximately equal to the speed of light c . Consequently, the expression simplifies to:

$$\frac{\sigma(p)}{p} \approx \frac{p^2}{m^2 L c} \cdot \sigma(T_{\text{fly}}) = \frac{\gamma^2 c}{L} \cdot \sigma(T_{\text{fly}}). \quad (3)$$

In the proposed KLM upgrade [11], accurate determination of the T_{fly} for a K_L meson relies on precise measurements of the start time (T_{start}) and stop time (T_{stop}). The majority of K_L mesons are produced directly at the interaction point (IP), and the T_{start} can be determined from the collision time at the SuperKEKB accelerator, which achieves a resolution better than 32 ps [25]. For

those originating from the decay of long-lived hadrons, such as B or D mesons, the lifetime of the parent meson is typically less than 10 ps [26]. Consequently, the expected resolution for T_{start} is projected to be better than 35 ps. The T_{stop} is determined using timing information from multiple hits within the hadronic cluster detected by the upgraded KLM system. Assuming a time resolution of 100 ps for T_{stop} and a typical flight distance of $L = 200$ cm from the IP to the new KLM in Belle II, the momentum resolution for a K_L meson with a momentum of 1.5 GeV/ c can achieve 0.2 GeV/ c , corresponding to a relative uncertainty of 13%. This enhanced four-momentum measurement improves studies of decay modes involving a K_L meson in the final state, such as $B^0 \rightarrow J/\psi K_L$, while also reducing accidental backgrounds in these processes. Additionally, there are cases where the momentum of a K_L cannot be determined solely from kinematic constraints, such as in $B^+ \rightarrow K^+ K_L K_L$. A new KLM with TOF measurement capability would enable such studies experimentally.

3. Improvements to the scintillation detector design

The current scintillation detection scheme in the KLM achieves a time resolution of only 1 – 2 ns, as demonstrated in laboratory tests [27]. This level of performance is insufficient for T_{fly} measurement, highlighting the necessity for an upgraded detection scheme. As we described for the new KLM detection scheme in the Belle II Upgrade CDR [11], several key improvements should be implemented for HTR.

- **Removal of WLS Fibers:** The WLS fibers in the scintillator were eliminated, and a thicker scintillator with a higher light yield and longer attenuation length was employed instead.
- **Design of New Preamplifiers:** High-bandwidth, low-noise SiPM front-end preamplifiers have been implemented to enhance the quality of the SiPM output signal.
- **Design of SiPM Array:** Large arrays of SiPMs have been utilized for photon collection. The rise time (τ_{rise}) of the signal from the SiPM array has been further decreased through a hybrid connection.
- **Dual-End Readout Scheme:** Drawing inspiration from TOF detector readout techniques, we have transitioned from a single-ended to a dual-end readout scheme, significantly improving time resolution at positions distant from the SiPM readout end.

For this study, we sourced plastic scintillators from two manufacturers: GaoNengKeDi Company [20] in Beijing and Saint-Gobain Company [28]. The BC420 scintillator from Saint-Gobain, known for its benchmark quality in TOF detectors, serves as a reference for evaluating cost-effective alternatives from GaoNengKeDi. The dimensions of the BC420 scintillator are $5\text{ cm} \times 3\text{ cm} \times 120\text{ cm}$, with a Bulk Light Attenuation Length (L_{Att}) of 110 cm [28]. In the past years, with the motivation for the R&D of Belle II KLM upgrade, our laboratory at Fudan University has been working closely with the GaoNengKeDi Company to improve the scintillators' quality, especially in the light yield and the L_{Att} . As illustrated in Fig. 2(a), we cataloged the GaoNengKeDi scintillators with dimensions ranging from $4\text{ cm} \times 2\text{ cm} \times 50\text{ cm}$ to $4\text{ cm} \times 2\text{ cm} \times 150\text{ cm}$ by the shipment date of the samples: GNKD_1, GNKD_2, GNKD_3, and GNKD_4. The BC420 scintillator is also depicted in Fig. 2(a). More information about these scintillators can be found in Table 1.

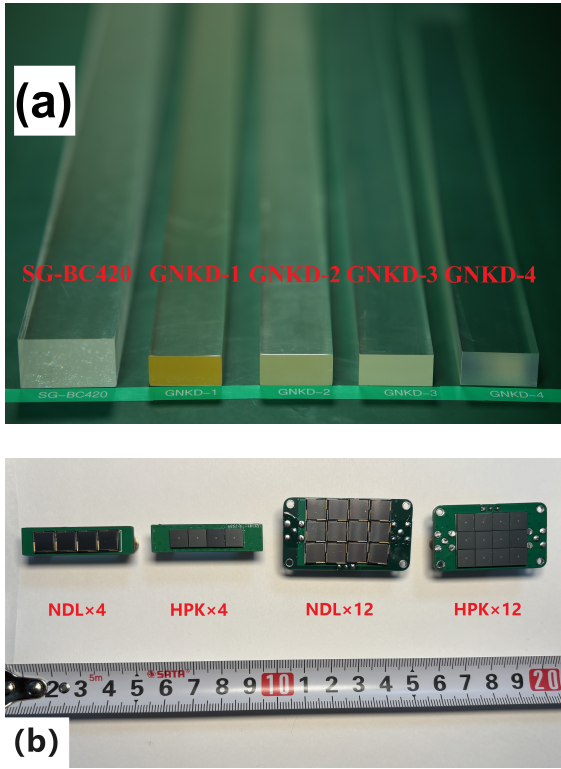


Figure 2: (a) BC420 scintillator sample from Saint-Gobain alongside various scintillator samples from GaoNengKeDi. (b) Different configurations of SiPM arrays with a preamplifier mounted on the back of the PCB.

All the SiPMs used in this study measure $6\text{ mm} \times 6\text{ mm}$, including the HPK S14160-6050 [29] and

the EQR20-11-6060 from Novel Device Laboratory (NDL) [30]. To further enhance the time resolution by increasing the photon collection area, we configure the multiple SiPMs into series, parallel, or hybrid arrangements, forming SiPM arrays [31], as illustrated in Fig.2(b).

Front-end electronics are essential for HTR measurements using a SiPM array. The front-end amplifier and SiPM array are mounted on the same printed circuit board (PCB) to minimize noise and interference during signal transmission. The preamplifier is designed using the ultra low noise, high bandwidth operational amplifier LMH6629 from Texas Instruments [32]. Our preamplifier provides a gain of +26 dB and a bandwidth of 426 MHz, enabling a τ_{rise} of 1 ns while reducing baseline noise to as low as 0.6 mV. A time resolution of 20 ps has been achieved using this preamplifier for SiPM [33].

4. Experimental setup for cosmic ray measurements

4.1. Experimental setup

We utilize cosmic rays to evaluate the HTR performance of the scintillator. Figure 3 shows the setup containing a trigger system including a logic board, the long scintillators from GaoNengKeDi or BC420 under test, SiPM arrays, and an oscilloscope for data acquisition (DAQ). The trigger system consists of two 10 cm strips (also from GaoNengKeDi) positioned at the top and bottom of the long scintillator(s) to determine the impact location and hit time of cosmic rays. Dual-end readouts collect photon data from both ends of a scintillator strip, enhancing the overall time resolution. This dual-end readout strategy is also applied to the triggers to mitigate the time walk effect caused by positional uncertainty in cosmic ray impacts. Notably, the trigger location is strategically placed at the midpoint of the elongated strip, where time performance is typically less accurate.

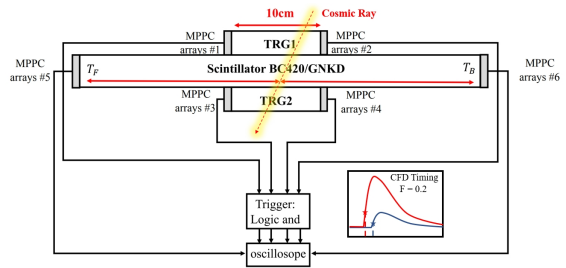


Figure 3: Experimental setup for cosmic ray testing of the scintillator.

We employ a Tektronix MSO58 oscilloscope with eight channels for the DAQ system. This oscilloscope features a sampling rate of 6.25 GS/s and an analog bandwidth of 1 GHz, meeting the requirements for high-speed signal digitization. For DAQ systems requiring more than eight channels, we use a CAEN desktop digitizer DT5742 [34]. This digitizer can handle 16 channels with a sampling rate of 5 GS/s and a bandwidth of 500 MHz.

The resulting data is processed offline on a computer after digitizing the waveform using the oscilloscope or digitizer. In the case of elongated strip-shaped scintillation detectors, significant variations in signal amplitude often occur due to fluctuations in photon collection or the distance from the hit position to the photosensors. To obtain accurate timing information, we apply the Constant Fraction Discrimination (CFD) method to the waveform, with the fraction set to $f = 0.2$.

4.2. Calculation of time resolutions

As shown in Fig. 3, the trigger system consists of two short scintillators with dimensions of $1 \text{ cm} \times 4 \text{ cm} \times 10 \text{ cm}$. Four SiPM arrays are mounted on the ends of the strips, with T_i ($i = 1, 2, 3, 4$) marking their recorded times. The hit times for the two strips are calculated as $T_{\text{trg1}} = (T_1 + T_2)/2$ and $T_{\text{trg2}} = (T_3 + T_4)/2$, and the trigger time T_0 (also the event T_0) is determined by $T_0 = (T_1 + T_2 + T_3 + T_4)/4$. To obtain the time resolution of T_0 [$\sigma(T_0)$], which is crucial for all HTR tests in this paper, we analyze the time difference between the two triggers, denoted as $\Delta T_{\text{trg}} = (T_1 + T_2)/2 - (T_3 + T_4)/2$. The distribution of ΔT_{trg} is fitted with a Gaussian function to determine its standard deviation $\sigma(\Delta T_{\text{trg}})$, from which we derive $\sigma(T_0) = \sigma(\Delta T_{\text{trg}})/2$. As described in Sec. 5.1, we obtain $\sigma(T_0) \approx 50 \text{ ps}$ for most of the cases. Furthermore, we can estimate the time resolution of one readout end to be $\sigma(T_i) \approx \sigma(\Delta T_{\text{trg}})$.

For a long strip under test, SiPM array#5 and array#6 are mounted on the two ends, with their recorded times denoted as T_F and T_B . The hit time on the long strip is calculated as $T_{\text{SC}} = (T_F + T_B)/2$. To determine the time resolution of this detector, we analyze the time difference $\Delta T = T_{\text{SC}} - T_0$. The distribution of ΔT is fitted with a Gaussian function to obtain its standard deviation $\sigma(\Delta T)$. By subtracting the uncertainty of T_0 , the time resolution of the long scintillator detector (LSD) is calculated via:

$$\sigma(T_{\text{LSD}}) = \sqrt{\sigma(\Delta T)^2 - \sigma(T_0)^2}. \quad (4)$$

5. Test results and analysis

5.1. Connection configurations of SiPM arrays

An array consists of four SiPMs to match the cross section of $1 \text{ cm} \times 4 \text{ cm}$ of a trigger strip. We investigate the time resolution using two connection configurations: parallel (4P) and series (4S). For long scintillators with larger cross sections, such as $4 \text{ cm} \times 2 \text{ cm}$ for GaoNengKeDi samples and $5 \text{ cm} \times 3 \text{ cm}$ for BC420, an extensive array of 12 SiPMs is required to ensure efficient light collection. To address this, we tested the arrays in three distinct connection configurations: pure series (12S), pure parallel (12P), and a hybrid of series and parallel (4S3P).

Connecting SiPMs in a pure parallel configuration increases the input junction capacitance of the amplifier, resulting in a slower τ_{rise} , larger baseline noise, and increased timing uncertainty. In contrast, connecting SiPMs in a pure series configuration effectively mitigates these issues. This arrangement significantly improves the τ_{rise} of the SiPM signal waveform, for example, reducing it from 12.4 ns in the 4P configuration to 4.1 ns in the 4S configuration, thereby enhancing time resolution. For the 12-SiPM arrays, the 12S configuration offers no significant advantage in τ_{rise} ; for instance, the τ_{rise} only marginally decreases from 4.1 ns in the 4S3P configuration to 4.0 ns in the 12S configuration. Meanwhile, a longer signal path for SiPM signals to reach the amplifier in the pure series configuration may degrade time resolution. Therefore, the 4S3P hybrid configuration is expected to be the optimized choice for an array of 12 SiPMs.

The overvoltage of the SiPM significantly impacts time resolution. Our test results indicate that increasing the overvoltage enhances the photon detection efficiency of the SiPMs, improves the signal-to-noise ratio (SNR), and subsequently boosts time resolution. However, excessively high overvoltage can significantly increase the dark count rate and crosstalk within the SiPM, reducing the SNR and negatively affecting time resolution. Therefore, selecting the appropriate overvoltage is critical for HTR.

The test results for HPK and NDL SiPMs as a function of the applied overvoltage are presented in Fig. 4. Figure 4(a) shows the performance of 4-SiPM arrays, revealing that the 4S configuration achieved superior time resolution compared to the 4P configuration. Notably, the HPK S14160-6050 outperformed the EQR20 SiPM from NDL in this regard. At the optimal overvoltage, the 4S configuration yielded a time resolution of $\sigma(\Delta T_{\text{trg}}) = 104 \pm 4 \text{ ps}$, corresponding to a calculated trigger system time resolution of $\sigma(T_0) = 52 \pm 2 \text{ ps}$.

The 4P and 4S configurations of HPK SiPMs and the 4S configuration of NDL SiPMs demonstrate stable time resolution across varying overvoltages. However, the time resolution of the 4P configuration of NDL SiPMs degrades significantly when the overvoltage is reduced from 5 V to 2.5 V. We choose the HPK 4S for the default trigger system. Figure 4(b) presents the results for 12-SiPM arrays, indicating that the hybrid 4S3P configuration achieved the best time resolution, with an optimal overvoltage of approximately 4 V.

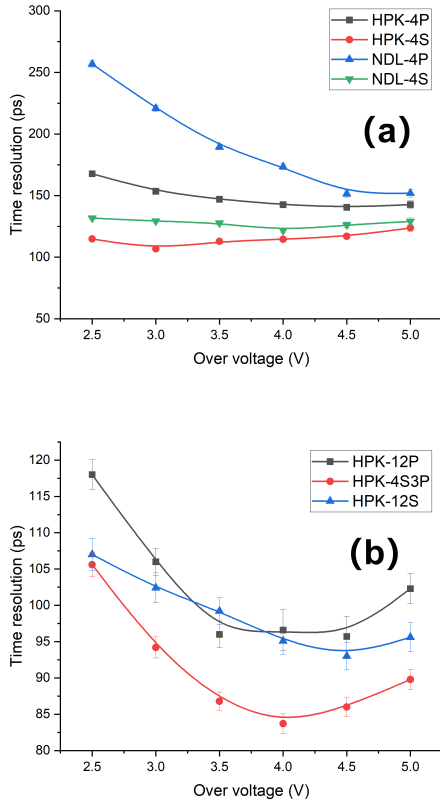


Figure 4: Comparison of configurations for SiPM arrays in (a) the trigger system and (b) the detector using BC420 scintillator and their impact on time resolution as a function of overvoltage.

5.2. Time resolution with single-end readout

By adjusting the positions of the upper and lower short triggers, we can evaluate the average signal amplitude and time resolution at various locations along the scintillator. This methodology enables determining a long scintillator's time resolution and L_{Att} across different positions. Figure 5 illustrates various scintillators' signal amplitude and time resolution at diverse hit

positions on the long strip. In this study, we use the readout from one end, i.e., the signal from array#5 and T_F in Fig. 3. T_0 is no longer suitable for determining the resolution of T_F . Instead, we use the left side of the trigger system, i.e., $T_{trgL} = (T_1 + T_3)/2$. The time difference $\Delta T_{single} = T_F - T_{trgL}$ mitigates the uncertainty due to the hit position in the trigger strips. We fit the distribution of ΔT_{single} with a Gaussian function to obtain its standard deviation $\sigma(\Delta T_{single})$. Then, the time resolution of T_F is calculated as:

$$\sigma(T_F) = \sqrt{\sigma(\Delta T_{single})^2 - \sigma(T_i)^2/2}. \quad (5)$$

The L_{Att} of a scintillator bar is determined by performing an exponential fit to the average amplitude of the SiPM signals shown in Fig. 5(a). To ensure the measured L_{Att} reflects the intrinsic attenuation length as accurately as possible, the influence of reflected light, which is more pronounced near the SiPM readout ends, is minimized by selecting data points located more than 50 cm from the readout end for fitting. This approach yields the following L_{Att} values for scintillators from different batches: 65 ± 9 cm for GNKD_1, 70 ± 2 cm for GNKD_2, 120 ± 7 cm for GNKD_3, and 82 ± 8 cm for BC420. Additional details are provided in Table 1. Due to the short length of the GNKD.4 scintillator (50 cm), its L_{Att} could not be measured well.

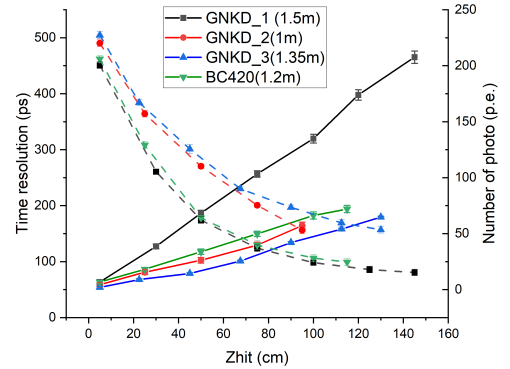


Figure 5: The variation of photon collection and single-ended time resolution is analyzed in relation to the position of cosmic ray hits. The photon collection and time resolution are represented in dashed lines and solid lines, respectively.

The time resolution strongly correlates with the number of photons collected by the SiPM array, as summarized in Table 1. All scintillators demonstrate excellent photon collection, exceeding 200 $p.e.$, and achieve excellent time resolutions of approximately 60 ps at the

Table 1: Comparison of photon collection and time resolution at the near-end and far-end of scintillators with different L_{Att} .

Type	$W \times H \times L$ (cm ³)	L_{Att} (cm)	Time Resolution (ps)		Collected Photons ($p.e.$)	
			$Z_{\text{hit}}=5$ cm	$Z_{\text{hit}}=95$ cm	$Z_{\text{hit}}=5$ cm	$Z_{\text{hit}}=95$ cm
SG-BC420	$5 \times 3 \times 120$	82 ± 8	63 ± 4	175 ± 6	206	30
GNKD_1	$4 \times 2 \times 150$	65 ± 3	63 ± 4	307 ± 8	200	26
GNKD_2	$4 \times 2 \times 100$	70 ± 9	59 ± 4	164 ± 6	220	53
GNKD_3	$4 \times 2 \times 135$	120 ± 7	53 ± 2	138 ± 6	227	70
GNKD_4	$4 \times 2 \times 50$	/	44 ± 3	$81 \pm 5(45 \text{ cm})$	341	154 (45 cm)

near end. As the hit position moves farther from the readout end, the number of photons collected by the SiPMs gradually decreases. Scintillators with larger L_{Att} and higher light yields, such as GNKD_3, exhibit superior time resolution. Despite this advantage, the time resolution of GNKD_3 degrades from 53 ± 2 ps at the near end to 140 ± 6 ps at the far end. These results underscore the necessity of implementing a dual-end readout scheme to maintain consistent performance across the entire length of the scintillator.

5.3. Time resolution with dual-end readout

The dual-end scheme averages the time information from both ends of the scintillator. The calculation of the time resolution of dual-end readouts at the midpoints of the scintillators has been explained in Sec. 4.2. For the time resolutions at other positions, we should take into account the amplitudes of the signals to avoid the large uncertainties due to the small light collections. We adopt a strategy similar to that used in TOF detectors [35], where the resolution of T_{SC} is determined by the weighted average of T_F and T_B :

$$T_{\text{SC}} = \frac{T_F \sigma_F^{-2} + T_B \sigma_B^{-2}}{\sigma_F^{-2} + \sigma_B^{-2}}, \quad (6)$$

$$\sigma_{T_{\text{SC}}}^{-2} = \sigma_F^{-2} + \sigma_B^{-2}, \quad (7)$$

with $T_F = T_0 + X/v$ and $T_B = T_0 + (L - X)/v$, where X is the distance from the cosmic ray hit position to the readout end, and v is the velocity of photon propagation in the scintillator.

The precision of T_{SC} is influenced by uncertainties in the muon hit position after weighted averaging, except the midpoint of the scintillator, where the weighting factors from both ends are nearly equal. Although a short scintillator with a length of 10 cm is used as the trigger, this dimension still introduces significant uncertainty in determining the hit position. One approach to reducing this uncertainty is to decrease the trigger length. However, this would substantially reduce the cosmic ray flux, resulting in a corresponding increase in measurement time. Each position must be tested over two weeks

to gather a statistically sufficient sample of more than 1,000 events. To address this challenge, we propose a multi-trigger testing scheme, as illustrated in Fig. 6(a). In this scheme, the trigger signals are shaped into different pulse widths ($\tau_1 = 50\text{ns}$, $\tau_2 = 100\text{ns}$, $\tau_3 = 150\text{ns}$) and input to the TR0 interface of the DT5742. During data analysis, the location of cosmic ray hits can be determined using these distinct pulse widths. This method enables simultaneous measurement of multiple positions, significantly improving the efficiency of the cosmic ray test.

To demonstrate the effectiveness of dual-end readout in improving the time resolution of a long scintillator detector, we conduct tests using the GNKD_3 scintillator. Figure 6(b) presents the results of the time resolution assessment with dual-end readout, alongside the single-end readout resolutions of T_F and T_B . We observe that the time resolution is least favorable at the center of the scintillator, measuring 70 ± 9 ps, while optimal resolution of approximately 50 ps is achieved at both ends. Notably, with dual-end readout, the position with the poorest time resolution typically occurs at the center, distinguishing it from single-end readout methodologies. Additionally, we compare the time resolution calculated using Eq. (6) with that derived from the weighted average of T_F and T_B . The results show a strong correlation between the two methods, validating the effectiveness of the dual-end readout approach.

Based on the insights gained from the test results, we can extrapolate the performance of longer scintillators. For example, in a scintillator with a length of 200 cm, which is a typical length of a long strip in the KLM detector, the position with the poorest time resolution occurs at the midpoint ($Z_{\text{hit}} = 100$ cm). Here, the time resolution for single-end readout is approximately 140 ± 6 ps for GNKD_3. By leveraging time information from both ends and averaging the data, the time resolution can be improved to $140/\sqrt{2} \approx 98$ ps.

In the tests on the scintillator samples from Gao-NengKeDi, the GNKD_4 scintillator demonstrates the best time resolution. It achieves an impressive time resolution of 44 ps at the near end and 81 ps at the far

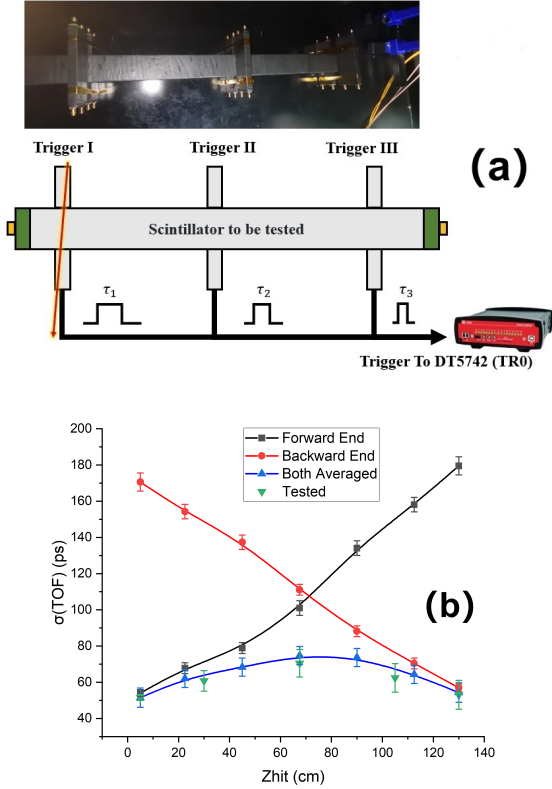


Figure 6: The measurement of time resolution for the GNKD.3 sample using cosmic ray hits is presented, where (a) illustrates the schematic diagram of the multi-trigger test system, and (b) shows the time resolution as a function of the scintillator position. The red and black lines represent the single-ended time resolution. The blue line corresponds to calculations using Eq. (6), while the green line depicts the time resolution results derived from the weighted average of times at both ends, with the trigger length reduced to 1 cm..

end, with a resolution better than 47 ps achieved through dual-end readout.

5.4. Measurement of cosmic ray velocity

An upgraded KLM should incorporate multiple layers to facilitate the reconstruction of hadronic clusters from K_L mesons or to track multiple hits from a muon track [11]. To simulate this application in our final experiment, we assemble an array using GaoNengKeDi scintillators to measure the average velocity of cosmic rays in our laboratory, which is situated on the third floor of an eight-story building. Due to the limited number of scintillator samples, we opted for 75 cm long scintillators from batch GNKD.1, which exhibited a consistent time resolution of 120 ± 5 ps, for constructing the prototype array.

The prototype apparatus is illustrated in Fig. 7(a). It comprises six parallel 75cm scintillator strips arranged vertically with an equal spacing of 7.5 cm. From top to bottom, these strips are labeled as SC1, SC2, SC3, SC4, SC5, and SC6. Two additional trigger strips are positioned at the top and bottom of the central region of the long strips. Dual-end readout is implemented for all eight strips to ensure precise timing measurements. Waveform acquisition is performed using the DT5742 digitizer, with the four channels of the trigger system generating logic signals that are routed into the TR0 input of the DT5742.

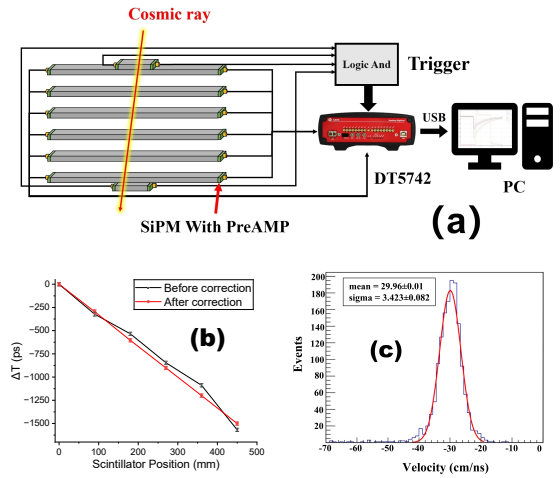


Figure 7: (a) Schematic of the prototype setup, featuring six long scintillators measuring $75 \text{ cm} \times 4 \text{ cm} \times 1.5 \text{ cm}$ and two short trigger scintillators measuring $10 \text{ cm} \times 4 \text{ cm} \times 1 \text{ cm}$. The distance between each pair of long scintillators is 7.5 cm. (b) Timing versus the position of the long scintillators for cosmic ray velocity measurements, comparing results before and after time calibration of the readout channels. (c) The Gaussian fit to the velocity distribution of all measured cosmic ray hits.

As shown in Fig. 7(b), the timing versus scintillator position for the six strips deviates from a straight line due to variations in the electronic readout channels. To address these variations, we perform a calibration using a pulsed laser. The laser is split into six beams, each directed to the middle position of the corresponding scintillator. By analyzing the timing discrepancies in the readouts, we identify variations primarily caused by electronic factors. We select SC1 as the reference channel and set $T_{\text{SC1}} = 0$ ps. The calibration constants for the other five channels are determined to be $T_{\text{SC2}} = 27$ ps, $T_{\text{SC3}} = -70$ ps, $T_{\text{SC4}} = -56$ ps, $T_{\text{SC5}} = -111$ ps, and $T_{\text{SC6}} = 68$ ps. After calibration, the timing versus scintillator position for the six strips aligns along a straight line, as shown in Fig. 7(b).

We then perform a linear fit of the timing versus position to determine the velocity in each event. Fitting the distribution of velocities yields an average velocity of 29.958 ± 0.011 cm/ns, with a standard deviation of 3.4 ± 0.1 cm/ns, as shown in Fig. 7(c). This corresponds to $\beta = 0.993$ and a momentum of 2.8 ± 0.7 GeV/c for muons in our laboratory. The measured velocity aligns with the expected average muon momentum of 3 – 4 GeV/c at the see level [36]. These results demonstrate the potential for improved HTR measurements with hits in multiple layers.

6. Conclusion and discussion

In this work, we present the R&D efforts for the KLM upgrade proposal of the Belle II experiment, focusing on the feasibility of accurately determining the momentum of neutral hadrons, such as K_L mesons and neutrons, through TOF measurements. Our R&D efforts centered on the development of a novel scintillator detector designed to enhance TOF capabilities. We explored the use of cost-effective plastic scintillators with large attenuation lengths, coupled with large-area SiPMs, to optimize photon collection efficiency.

Through extensive testing, we developed new scintillator materials and integrated compact $6 \text{ mm} \times 6 \text{ mm}$ SiPM arrays, achieving significant improvements in performance. Various developing scintillators were evaluated. Notably, the 135 cm-long sample demonstrated a bulk attenuation length of 120 ± 7 cm and a time resolution of 70 ± 7 ps at its midpoint. Additionally, the latest 50 cm scintillator achieved an exceptional time resolution of 47 ± 2 ps.

To validate the applicability of this technology in the Belle II experiment, we constructed a prototype detector and successfully measured cosmic ray velocities, obtaining a value of 29.958 ± 0.011 cm/ns, corresponding to a muon momentum of 2.8 ± 0.7 GeV/c in our laboratory. These results highlight the potential of the proposed detector design to significantly improve neutral hadron momentum measurements in an upgraded Belle II KLM system. Future work will focus on scaling up the prototype and further optimizing its performance for integration into the Belle II experiment.

According to Eq. (3), improving $\sigma(T_{\text{fly}})$ is essential for achieving better momentum resolution. Below, we outline several strategies to enhance the TOF capability of an upgraded KLM in Belle II:

- **Use shorter strips:** The 50 cm GNKD_4 sample demonstrated a time resolution of 47 ± 2 ps, significantly better than the 70 ± 7 ps resolution of

the 135 cm GNKD_3 sample. This improvement is attributed to the compact photon detection system utilizing SiPMs, which minimizes dead zones while maintaining high performance.

- **Employ multiple detector layers:** By utilizing N layers of the detector, the time resolution can be improved by a factor of $1/\sqrt{N}$ due to statistical averaging. This would be useful for the time information from a single track.
- **Optimize the algorithm for determining T_{stop} :** Advanced algorithms, particularly those leveraging fast-developing AI technologies, would improve the extraction of T_{stop} from hadronic clusters in the upgraded KLM.

These strategies collectively offer promising pathways to improve $\sigma(T_{\text{fly}})$ and, consequently, the overall momentum resolution of the detector.

During the preparation of this work, the authors used DeepSeek and ChatGPT to improve language and readability. After using these tools, the authors reviewed and edited the content as needed and take full responsibility for the content of the publication.

References

- [1] A. Airapetian *et al.* [ATLAS], CERN-LHCC-99-15.
- [2] G. L. Bayatian *et al.* [CMS], J. Phys. G **34** (2007) no.6, 995-1579
- [3] N. Ali *et al.*, J. Instrum. **15** (2020) P09016.
- [4] CMS Collaboration, J. Instrum. **5** (2010) T03012.
- [5] B. Aubert *et al.* (BABAR Collaboration), Nucl. Instrum. Methods A **479** (2002) 1.
- [6] A. Abashian *et al.* (Belle Collaboration), Nucl. Instrum. Methods A **479** (2002) 117.
- [7] T. Abe *et al.*, KEK Report 2010-1, arXiv:1011.0352.
- [8] I. Adachi *et al.*, Nucl. Instrum. Methods A **907** (2018) 46.
- [9] M. Ablikim *et al.* (BESIII Collaboration), Nucl. Instrum. Methods A **614** (2010) 345.
- [10] E. Kou *et al.*, Prog. Theor. Exp. Phys. **2019** (2019) 123C01.
- [11] H. Aihara *et al.*, *The Belle II Detector Upgrades Framework Conceptual Design Report*, arXiv: 2406.19421v1.
- [12] F. Forti (for Belle II Collaboration), *Snowmass Whitepaper: The Belle II Detector Upgrade Program*, arXiv:2203.11349v1.
- [13] H. Kichimi *et al.*, Nucl. Instrum. Methods A **453** (2000) 315.
- [14] Y. K. Heng *et al.*, IEEE Nucl. Sci. Symp. Conf. Rec. (2007): 53-56.
- [15] W.J. Llope *et al.*, Nucl. Instrum. Methods A **241** (2005) 306.
- [16] A. Alici *et al.*, Nucl. Instrum. Methods A **706** (2013) 29.
- [17] P. Cao *et al.*, Nucl. Instrum. Methods A **953** (2020) 163053.
- [18] M. Böhm *et al.*, J. Instrum. **11** (2016) C05018.
- [19] C. Chung, Instruments **6** (2022) 14.
- [20] GNKD website, <http://www.gaoenkedi.com/>
- [21] T. Aushev *et al.*, Nucl. Instrum. Methods A **789** (2015) 134
- [22] Kuraray, Ltd. (Japan), <https://www.kuraray.com/products/psf>[Accessed 12 JAN 2024]
- [23] BelleII VR, <http://www1.phys.vt.edu/~piilonen/VR/>

- [24] S. Agostinelli *et al.*, Nucl. Instrum. Methods A **506** (2023) 250;
J. Allison *et al.*, Nucl. Instrum. Methods A **835** (2016) 186.
- [25] A. Kazunori *et al.*, Nucl. Instrum. Methods A **907** (2018) 188
- [26] S. Navas *et al.* (Particle Data Group), Phys. Rev. D **110** (2024) 030001.
- [27] H. Y. Zhang *et al.*, J. Instrum. **19** (2024) P06020.
- [28] BC418-420-422 Datasheet, <https://luxiumsolutions.com/sites/default/files/2021-09/BC418-420-422%20Data%20Sheet>.
- [29] Hamamatsu MPPC website,
https://www.hamamatsu.com/eu/en/product/optical-sensors/mppc/mppc_mppc-array.html
- [30] NDL, <http://www.ndl-sipm.net/>
- [31] T. Cervi *et al.*, Nucl. Instrum. Methods A **912** (2018) 209.
- [32] LMH6629 Datasheet, <https://www.ti.com/product/LMH6629>
- [33] X. Y. Wang *et al.*, Nucl. Sci. Tech. **34** (2023) 169
- [34] DT5742 16+1 Channel 12 bit 5 GS/s Switched Capacitor Digitizer, <https://www.caen.it/products/dt5742/>
- [35] S. L. Li *et al.*, Chin. Phys. C **37** (2013) 016003.
- [36] R. Bellotti *et al.*, Phys. Rev. D **35** (1996) 53.